J. Fluid Mech. (1992), *vol.* 236, *pp.* 27–42
Printed in Great Britain

The thermal bar

By S. S. ZILITINKEVICH, K. D. KREIMAN AND A. YU. TERZHEVIK

Institute of Limnology, Academy of Sciences of the USSR, 196199, St Petersburg, USSR

(Received 5 November 1989 and in revised form 15 August 1991)

A simple theoretical model of the thermal bar is derived on the basis of heat budget equations for the following three zones of a wedge-shaped water basin warmed from above: (i) stably stratified shallow warm-water zone; (ii) vicinity of the bar; (iii) convectively mixed deep cold zone. In contrast to the traditional approach, advective warming of the vicinity of the bar and associated facilitating of the thermal bar propagation are taken into account. Theoretical predictions are compared with the data of lacustrine and laboratory measurements taken from current literature. New laboratory experiments have been carried out to examine the laminar regime of the thermal bar.

1. Introduction

The nature of the thermal bar is as follows. In spring, after the ice breaks in lakes, water warming starts. The heat flux passing into the water is determined mainly by meteorological factors. It varies comparatively weakly in the horizontal direction. Therefore the shallow near-shore zone of a water body is heated quicker than the offshore deep-water zone. The temperature field becomes horizontally inhomogeneous. Owing to the singularity of the equation of state of fresh water, stratification of density on both sides of the isotherm $T = T_m$, corresponding to the maximum density, appears to show opposite behaviour: hydrostatically stable in the shallow zone and unstable in the deep-water zone. In the vicinity of the isotherm $T = T_m$ double-cell convection develops with a heavy descending current in the narrow zone between the cells. The related frontal interface is called the *thermal bar*. In the course of warming of the reservoir, the thermal-bar region is displaced further from the shore. This process proceeds until the temperature of the cold deep-water zone reaches the value of T_m.

A similar phenomenon may be observed during autumn if the weather is calm: the shallow near-shore zone is cooled quicker than the offshore deep-water zone. Its temperature drops below the temperature of density maximum earlier. Further cooling of the lake, maintaining the thermal convection regime in the deep-water zone, leads to the establishing of hydrostatically stable stratification in the shallow water. The descending current, i.e. the thermal bar, also occurs in the vicinity of the isotherm $T = T_m$.

The phenomenon was discovered more than a hundred years ago by Forel (1880). He observed it in Lake Leman and gave a quite correct qualitative explanation of its physical nature. The term itself, *thermal bar*, belongs to Forel too. For almost half a century this phenomenon remained in oblivion. Interest in it was revived by Tikhomirov (1959, 1963, 1982) who was the first to study the thermal-bar region in detail, using hydrological measurements, aerial photographs and chemical analysis of lake water samples. At present, the main source of information on thermal bars in

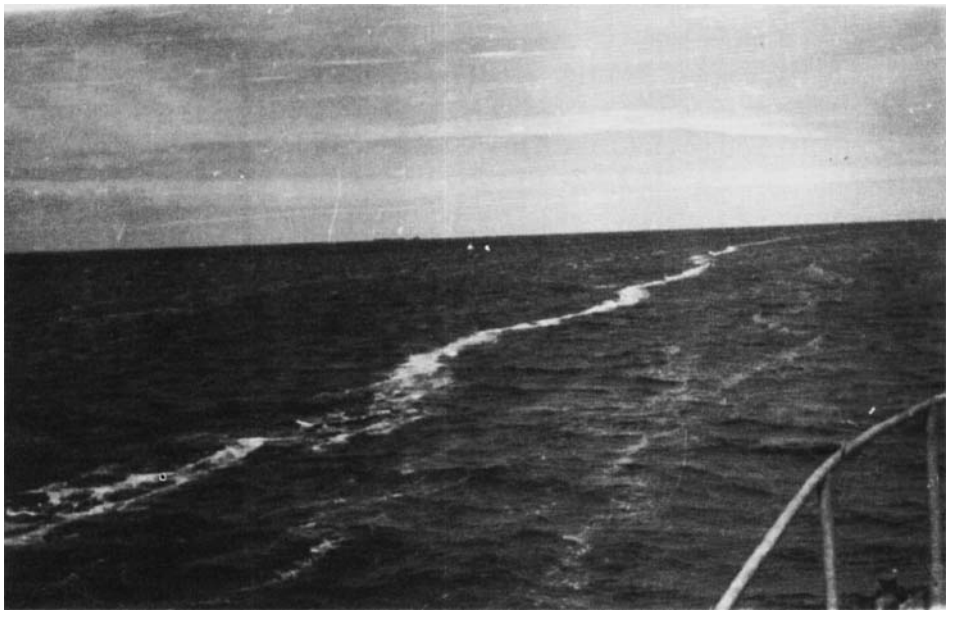

FIGURE 1. The thermal bar in Lake Ladoga, 30 May 1959 (photograph by Tikhomirov).

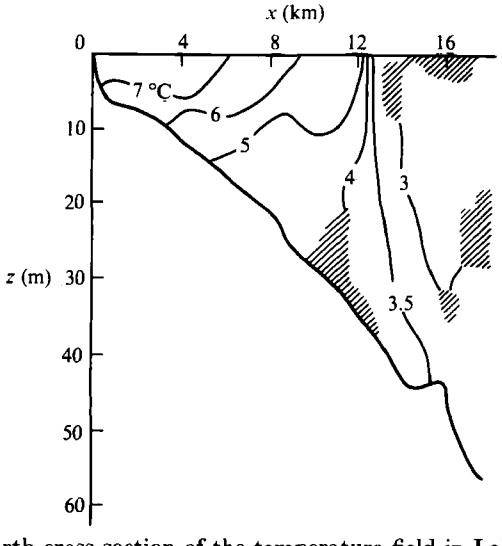

FIGURE 2. South–north cross-section of the temperature field in Lake Ontario early May, 1965, after Rodgers (1966).

the USSR lakes is his book (Tikhomirov 1982). He observed that the near-bottom horizontal currents spread sideways from the bar, while the near-surface ones converge towards it. This latter phenomenon often makes the bar line visible to the naked eye: it collects surface flakes of foam, plankton, water plants and pollution films. A photograph of such a line on the surface of Lake Ladoga is shown in figure 1. Since the mid-1960s experimental studies of thermal bars have been carried out by American and Canadian groups in the Great Lakes of North America (Rodgers 1966, 1968). A temperature section of Lake Ontario is shown in figure 2.

Experiments on modelling thermal bars have been performed in a wedge-shaped

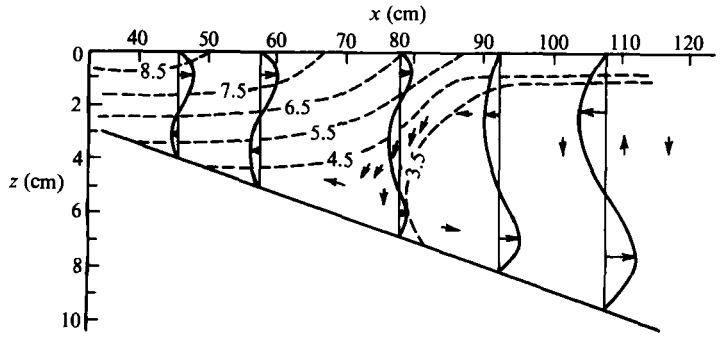

FIGURE 3. Distribution of temperature and current velocities in the laboratory experiment on a thermal bar, after Elliott & Elliott (1970). The dashed curves denote isoterms (°C); the solid lines, horizontal velocity profiles. The arrows show distances travelled by fluid particles per minute.

laboratory tank (Elliott & Elliott 1969, 1970). Figure 3 presents distributions of temperature and current velocities from these. Comparing it with figure 2, it is easy to notice the general similarity between the laboratory and lacustrine isotherm pictures.

Not many theoretical investigations of thermal bars have been carried out. Numerical models have been proposed (Csanady 1970; Huang 1972; Bennett 1971), based on two-dimensional momentum and heat-transfer equations, including nonlinear advective terms and turbulent exchange terms. The latter were expressed by means of horizontal and vertical turbulent viscosities and turbulent heat conductivities. Fitting of these coefficients allowed the temperature and current velocity fields to be obtained (Bennett 1971). Attempts were also made to explain the temperature regime during bar development by considering different versions of one-dimensional heat-transfer equations (Elliott & Elliott 1970; Elliott 1971; Sundaram 1974).

The main question which should be answered by a theoretical model of the thermal bar is: how does the front displacement proceed? A quite clear, though very approximate approach was proposed by Elliott & Elliott (1970), Elliott (1971) and Tikhomirov (1982). We consider the derivation as it applies to spring warming. The deep-water cold part of a lake situated in front of the thermal bar is involved in convection. It is assumed to be well-mixed. The water temperature there is depth-constant, and horizontal heat transport due to advection and turbulent exchange is insignificant. In this case, the heat transfer equation is easily integrated (see §2). Using the natural condition of no heat flux through the bottom, the solution of the equation is

$$T - T_0 = Q_s t/D(x) = Q_s t/\mu x, \tag{1}$$

where t is time, T is temperature, T_0 is its initial value, D is depth at distance x from the shore, and Q_s is kinematic heat flux through the water surface assumed independent of t and x. The second equality in (1) corresponds to the case when the tangent of the bottom inclination angle, $\mu = D(x)/x$, is independent of x. According to (1), the position of the thermal bar at a particular time, i.e. the distance of $x = l$ from the shore to the isotherm $T(x) = T_m$, is expressed by

$$l = Q_s t/(T_m - T_0)\mu. \tag{2}$$

The main drawback of the approach seems to be that it overlooks the warming action of the warm, shallow-zone water on the thermal conditions in the vicinity of

the bar. Indeed, the descending convective jet associated with the bar leads to entrainment and consequently to penetration of warm water through the back side of the bar. It may serve as an additional heat supply to the bar zone and thus facilitate the displacement of the bar towards greater depths. A theoretical model taking this mechanism into account was suggested by Zilitinkevich & Terzhevik (1987, 1989) and Zilitinkevich & Kreiman (1990). Further development of the problem is given in the present paper.

We will consider the simplest two-dimensional problem in a straight-line, wedge-shaped basin concentrating on the above-mentioned effect of dynamic warming on the acceleration of thermal bar propagation. Secondary effects, like the consequences of complicated geometry of a basin, possible action of the Coriolis force (in sufficiently large lakes), etc. will not be taken into account.

It is desirable, at the same time, to consider in general the possibility of relating the empirical data taken from field measurements to that from laboratory experiments. That is why we will try to examine some specific features of the laminar thermal bar. The problem is that the convective jet forming the bar in laboratory tanks must be definitely laminar during a certain initial period of the experiment. Therefore the thermal bar in laboratory and the same bar in a natural water body are phenomena of a different nature, generally speaking. Is it possible to reproduce the turbulent bar in the laboratory? If it is, then how can the periods of laminar and turbulent regimes be distinguished? Without answers to these questions, laboratory modelling is of very little use.

2. Heat regimes of different zones

We consider time-constant and horizontally homogeneous heating of water filling a wedge-shaped basin whose cross-section is shown on figure 4. Here the z-axis is directed vertically downwards and the x-axis horizontally from the shore (i.e. the sharp edge of the wedge) perpendicular to the shoreline. Homogeneity is assumed along the other horizontal.

As already explained in §1, after switching on the heater, the water temperature starts rising more quickly in the shallow than in the deep part of the basin. As a result, currents develop. If the initial temperature is below T_m, then a thermal bar develops too. Its position is displaced gradually towards greater depths. So, at each moment of time three zones are distinguishable in the basin: 'W', the stably stratified shallow warm-water zone ($0 < x < l$); 'C', the deep cold-water zone involved in three-dimensional convection ($l+\Delta l < x < L$); 'B', the bar zone between them ($l < x < l+\Delta l$). These zones are represented in figure 4 by segments OW′W″, B′C′C″B″, W′B′B″W″.

We take the bar zone to be a subregion of our wedge whose mean temperature, T_B, is equal to the temperature of maximum density, T_m; while its width, Δl, makes up a standard portion of the local depth, μl. The latter statement reflects the fact that the basin depth is the appropriate scale for the convection circulation cells both in the vertical and horizontal directions. Such a definition is expressed mathematically as

$$T_B = T_m, \quad l+\Delta l = Ml, \tag{3}$$

where M is a dimensionless parameter:

$$M = 1+C_M\mu; \tag{4}$$

C_M is a dimensionless constant. Its choice will be discussed below.

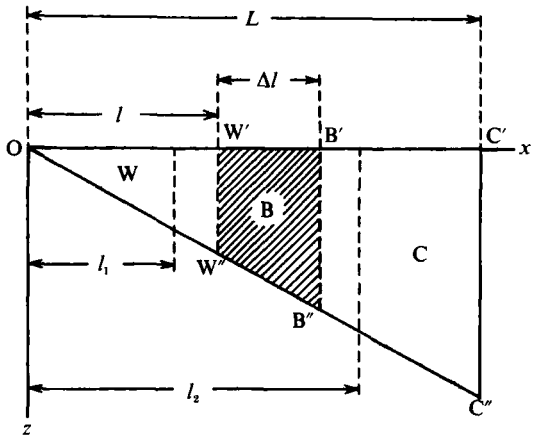

FIGURE 4. Cross-section of a wedge-shaped basin. See text for details of the labelling.

Assuming homogeneity of the temperature field along the shoreline, the heat transfer equation becomes

$$\frac{\partial T}{\partial t}+u\frac{\partial T}{\partial x}+w\frac{\partial T}{\partial z}=-\frac{\partial Q}{\partial z}, \tag{5}$$

where u and w are components of the current velocity along the horizontal and vertical axes x and z, Q is the vertical kinematic heat flux.

We adopt the initial condition

$$T=T_0<T_m \quad \text{at} \quad t=0 \tag{6}$$

and boundary conditions

$$Q=Q_s \quad \text{at} \quad z=0, \quad Q=0 \quad \text{at} \quad z=\mu x; \tag{7}$$

the second of these conditions means that there is no heat flux through the bottom.

The velocity components must satisfy the continuity equation:

$$\frac{\partial u}{\partial x}+\frac{\partial w}{\partial z}=0, \tag{8}$$

the condition of a no-slip boundary at the bottom:

$$w=u=0 \quad \text{at} \quad z=\mu x, \tag{9}$$

and the condition of a stress-free boundary on the water surface:

$$w=0 \quad \text{at} \quad z=0. \tag{10}$$

The latter condition is taken here in the form which corresponds to neglecting deviations of the water level from its equilibrium state.

If we assume temperature to be constant with depth and neglect advective terms in (5), then the solution of the problems (5)–(7) will be a temperature field given by (1). Such an approximation is suitable for the cold convective zone C but obviously unsuitable on the other side of the bar, in the warm stratified zone W.

We introduce, first, the averaging operator over a region G, namely the part of our wedge bounded on two sides by verticals $x=l_1(t)$ and $x=l_2(t)$:

$$\Pi_G(f)=\frac{2}{\mu(l_2^2-l_1^2)}\int_{l_1}^{l_2}\mathrm{d}x\int_0^{\mu x}f\,\mathrm{d}z, \tag{11}$$

and, secondly, the averaging operators along these verticals:

$$\Pi_i(f) = \frac{1}{\mu l_i}\int_0^{\mu l_i} f(l_i, z, t)\,\mathrm{d}z; \quad i = 1, 2, \tag{12}$$

where $f = f(x, z, t)$ is a certain function.

Applying the operator (11) to (5) and taking into account (7)–(10), we obtain

$$\tfrac{1}{2}(l_2^2 - l_1^2)\frac{\mathrm{d}T_\mathrm{G}}{\mathrm{d}t} + (T_1 - T_\mathrm{G})\,l_1\frac{\mathrm{d}l_1}{\mathrm{d}t} + (T_\mathrm{G} - T_2)\,l_2\frac{\mathrm{d}l_2}{\mathrm{d}t} = (l_2 - l_1)\frac{Q_\mathrm{s}}{\mu} + F_1 l_1 - F_2 l_2, \tag{13}$$

where T_G is temperature averaged over the G-region, T_1 and T_2 are temperatures averaged along verticals $x = l_1$ and $x = l_2$, and F_1 and F_2 are dynamic horizontal heat fluxes through these verticals:

$$T_\mathrm{G} = \Pi_\mathrm{G}(T), \quad T_i = \Pi_i(T), \quad F_i = \Pi_i(uT); \quad i = 1, 2. \tag{14a–c}$$

Using (13), it is easy to derive equations to predict the mean temperature of the whole basin, $\bar{T}$, and the mean temperatures of the warm and cold zones, T_W and T_C, as well as the heat balance equation of the bar zone, whose temperature, $T_\mathrm{B} = T_\mathrm{m}$, is constant.

Indeed, assuming $l_1 = 0$, $l_2 = L$, we transform G into the whole wedge under consideration, so that (13) converts into the equation for the mean basin temperature:

$$\frac{L}{2}\frac{\mathrm{d}\bar{T}}{\mathrm{d}t} = \frac{Q_\mathrm{s}}{\mu}. \tag{15}$$

Assuming $l_1 = 0$, $l_2 = l$, we transform G into W and obtain from (13) the following equation for the mean temperature of the warm zone:

$$\frac{1}{2}\frac{\mathrm{d}T_\mathrm{W}}{\mathrm{d}t} = \frac{Q_\mathrm{s}}{\mu} - F_l - (T_\mathrm{W} - T_\mathrm{m})\frac{\mathrm{d}l}{\mathrm{d}t}. \tag{16}$$

Here the bar-zone temperature, $T_\mathrm{B} = T_\mathrm{m}$, is substituted into the right-hand side for the temperature, T_l, averaged along the vertical $x = l$; F_l is dynamic heat flux through this vertical. In the context of the above-stated definition of what we understand as the bar zone B, the approximation

$$T_l \approx T_\mathrm{B} = T_\mathrm{m}, \tag{17}$$

used in (16), can be interpreted as a condition which specifies the choice of the dimensionless constant C_M.

In a similar way one can easily derive the equation of the bar-zone heat balance:

$$0 = (M-1)\frac{Q_\mathrm{s}}{\mu} + F_l - MF_{l+\Delta l} - [(T_l - T_\mathrm{m}) + M^2(T_\mathrm{m} - T_{l+\Delta l})]\frac{\mathrm{d}l}{\mathrm{d}t}, \tag{18}$$

and the equation for the cold-zone mean temperature:

$$\tfrac{1}{2}(L^2 - M^2 l^2)\frac{\mathrm{d}T_\mathrm{C}}{\mathrm{d}t} = (L - Ml)\frac{Q_\mathrm{s}}{\mu} + MlF_{l+\Delta l} - M^2(T_{l+\Delta l} - T_\mathrm{C})\,l\frac{\mathrm{d}l}{\mathrm{d}t}, \tag{19}$$

where $T_{l+\Delta l}$ is the temperature averaged along the vertical $x = l + \Delta l$, $F_{l+\Delta l}$ is the dynamic heat flux through this vertical.

The mean temperatures under consideration must satisfy the requirement of a net heat balance:

$$L^2\bar{T} = l^2T_W + (M^2-1)\,l^2T_m + (L^2-M^2l^2)\,T_C. \tag{20}$$

So only three of the equations (15), (16), (18), (19) are independent.

Integrating the continuity equation (8) from the surface to the bottom, taking due account to the boundary conditions (9) and (10), we find that the total current through any vertical section $x = l_i$ is equal to zero:

$$\int_0^{\mu l_i} u\,dz = 0. \tag{21}$$

Therefore, if temperature does not change with depth, the dynamic heat flux F_i is also equal to zero, according to its definition given by (14*c*). The bar zone B is temperature-homogeneous. The adjoining cold zone C is well-mixed in the vertical direction owing to convection, so that temperature here is depth-constant. Hence, temperature is also depth-constant at the interface between B and C (at $x = l+\Delta l$), i.e. the dynamic heat flux through the interface is negligible:

$$F_{l+\Delta l} = 0. \tag{22}$$

The approximate vertical homogeneity of temperature in zones C and B can be seen in the empirical temperature sections (figures 2 and 3). Also, the dynamic transport across the thermal bar was estimated as negligibly small from observations of natural tracers (Hubbard & Spain 1973): when fluorescent water was added to inflows, fluorescence appeared in the stably stratified shallow zone and probably also the bar zone, but practically none penetrated into the convectively mixed, deep-water zone.

By virtue of (22) the heat regime of zone C can be considered independently of the remaining part of the basin. This means that the temperature distribution in C is described by (1). Its averaging over the whole zone C gives

$$T_C = T_0 + 2Q_s\,t/(L+Ml)\,\mu. \tag{23}$$

This expression satisfies the reduced version of (19) at $F_{l+\Delta l} = 0$.

Equation (15), maintaining the initial condition $\bar{T} = T_0$ at $t = 0$, gives

$$\bar{T} = T_0 + 2Q_s\,t/L\mu. \tag{24}$$

We substitute (3), (4), (23), (24) into (20) to obtain

$$T_W - T_m = 2MQ_s\,t/l\mu - M^2(T_m - T_0). \tag{25}$$

It now remains to determine the dynamic heat flux F_i. Then the system of equations (16), (25) will be closed.

The initial condition for l is

$$l = 0 \quad \text{at} \quad t = 0, \tag{26}$$

which means that the thermal bar originates at the shore edge.

3. Horizontal dynamic heat flux

According to figures 2 and 3 and all other available experimental data (Rodgers 1966, 1968; Elliott & Elliott 1969, 1970; Tikhomirov 1982), isotherms are more or less horizontal within the stably stratified warm zone W almost to the boundary with the bar zone B. It is evident that the strong hydrostatic stability in W is manifested

in the suppression of the vertical turbulent exchange, while the horizontal advective transport appears to be, on the contrary, forced. As a result, some sort of complete mixing takes place in the horizontal plane. If so, then near the interface between W and B, the scales of both vertical and horizontal temperature differences are

$$\delta T_{\rm v} = \delta T_{\rm h} = T_{\rm W} - T_{\rm m}. \tag{27}$$

The horizontal dynamic heat flux, F_l, is generated by penetration of water from W into B. It can be estimated as proportional to the horizontal temperature difference scale, $\delta T_{\rm h}$, and the descending-current velocity scale, w. That is why for either a turbulent or laminar regime the following expressions are valid:

$$F_l = \begin{cases} C_t w \delta T_{\rm h} & (28) \\ C_l w \delta T_{\rm h}, & (29) \end{cases}$$

where C_t and C_l are different dimensionless constants, both known to be much less than unity (see Turner 1973, chapter 8; Golitsyn 1980).

Now we have to determine the vertical velocity scale, w. We use the quadratic form of the equation of state for fresh water:

$$\rho = \rho_{\rm m}[1 - \tfrac{1}{2}a(T - T_{\rm m})^2], \tag{30}$$

where ρ is water density, $\rho_{\rm m}$ is its maximum value corresponding to the temperature $T_{\rm m} = 277$ K, $a = 1.65 \times 10^{-5}$ K^{-2}. Taking into account (30), the characteristic scale of the buoyancy acceleration, g', is defined in terms of the vertical temperature difference:

$$g' = ga\delta T_{\rm v}^2, \tag{31}$$

where g is gravitational acceleration.

In the *turbulent regime*, the assumption of a balance between buoyancy and inertia forces in the momentum equation together with (31) lead to

$$w = (ga\mu l)^{\frac{1}{2}} \delta T_{\rm v}. \tag{32}$$

Then, using (27) and (28), the horizontal dynamic heat flux is expressed as

$$F_l = C_t (ga\mu l)^{\frac{1}{2}} (T_{\rm W} - T_{\rm m})^2. \tag{33}$$

In the *laminar regime*, the vertical velocity scale, w, is evaluated from the alternative assumption of a balance between buoyancy and viscosity forces, once again using (31), resulting in the following expression:

$$w = (ga/\nu)(\mu l)^2 \delta T_{\rm v}^2 \tag{34}$$

and then, using (27) and (29),

$$F_l = C_l (ga/\nu)(\mu l)^2 (T_{\rm W} - T_{\rm m})^3. \tag{35}$$

A generally equivalent assumption of a balance between the convective generation of kinetic energy and its viscous dissipation was used by Golitsyn (1980) to derive the following expression for w in the general case of laminar convection:

$$w = \frac{\kappa}{a_w d} (Ra\, Nu)^{\frac{1}{2}}. \tag{36}$$

Here $a_w \approx 9$ is non-dimensional constant, κ is molecular heat conductivity, d is the liquid layer thickness, Ra and Nu are the Raleigh number and Nusselt number, respectively:

$$Ra = \frac{g' d^3}{\kappa \nu}, \quad Nu = \frac{F_l d}{\kappa \delta T_{\rm h}}, \tag{37a, b}$$

ν is molecular viscosity. Applying (36) and (37) to our case, i.e. substituting therein $d = \mu l$ and $F_l = C_l w \delta T_h$, we immediately obtain (34).

It is known that a laminar convection regime is replaced by a turbulent regime when the Raleigh number exceeds a certain critical value, Ra_t. In the case of convection above a heated surface this value is $14000 Pr^{0.6}$, where $Pr = \nu/\kappa$ is the Prandtl number (Turner 1973, chapter 7). Hence for water Ra_t is of order 10^6.

According to (37*a*), the condition for a thermal bar becoming turbulent is when it is beyond the following critical depth:

$$d_t = \left[\frac{Ra_t \nu\kappa}{ga(T_w - T_m)^2}\right]^{\frac{1}{3}}. \tag{38}$$

Taking $Ra_t \approx 10^6$ and $(T_w - T_m) \approx 4$ K, (38) gives a tentative estimate of d_t of the order of a few centimetres. So the answer to the first question raised at the end of the Introduction is obtained: the turbulent regime of the thermal bar can definitely be realized in the laboratory.

4. Propagation of the bar

In the previous sections we derived two alternative closed systems of equations in the unknown variables: l, T_w and F_l, namely (16), (25), (33) for the turbulent regime of a thermal bar and (16), (25), (35) for its laminar regime. Both systems are to be solved under the initial condition (26).

4.1. *Turbulent regime*

We use the external parameters Q_s, ga, μ, $T_m - T_0$ to compile the following length- and timescales:

$$l_* = \frac{Q_s^2}{ga\mu^3(T_m - T_0)^4}, \quad t_* = \frac{Q_s}{ga\mu^2(T_m - T_0)^3}. \tag{39}$$

Physically, l_* is the characteristic distance covered by the thermal bar during the characteristic period t_*. According to (39), the displacement-rate scale of a thermal bar appears to be equal to $l_*/t_* = Q_s/\mu(T_m - T_0)$, which is the same scale as implied in (2).

We introduce dimensionless variables:

$$\tau = t/t_*, \quad \lambda = l/l_*, \quad \theta = (T_w - T_m)/(T_m - T_0), \quad \Phi = F_l/Q_s. \tag{40}$$

Equations (16), (25) and (33) take the form

$$\frac{\lambda}{2}\frac{d\theta}{d\tau} = 1 - \theta\frac{d\lambda}{d\tau} - \Phi, \quad \Phi = C_t^{\frac{1}{3}}\lambda^2\theta^2, \tag{41*a*, *b*}$$

$$\theta = 2M\frac{\tau}{\lambda} - M^2, \quad M = 1 + C_M\mu. \tag{42*a*, *b*}$$

The problem of thermal-bar propagation is reduced to integrating the equation

$$\left(M - \frac{\tau}{\lambda}\right)\frac{d\lambda}{d\tau} - C_t M\lambda^{\frac{1}{3}}\left(2\frac{\tau}{\lambda} - M\right)^2 - \frac{M-1}{M} = 0 \tag{43}$$

under the initial condition

$$\lambda = 0 \quad \text{at} \quad \tau = 0. \tag{44}$$

The solution of the problem has the following asymptotes at $\tau \ll C_t^{-2}$:

$$\lambda \sim \frac{2M-1}{M^2}\tau + \frac{2C_t M}{(5M-3)(2M-1)^{\frac{1}{2}}}\tau^{\frac{3}{2}}, \tag{45}$$

$$\theta \sim \frac{M^2}{2M-1} - \frac{4C_t M^6}{(5M-3)(2M-1)^{\frac{5}{2}}}\tau^{\frac{1}{2}}, \tag{46}$$

and at $\tau \gg C_t^{-2} \times 10^{-1}$:

$$2\tau \sim M\lambda + C_t^{-\frac{1}{2}} M^{-1} \lambda^{\frac{3}{4}}, \tag{47}$$

$$\theta \sim C_t^{-\frac{1}{2}} \lambda^{-\frac{1}{4}}. \tag{48}$$

These expressions show the following behaviour of the solution: in the course of time, the dimensionless rate of bar displacement, $\mathrm{d}\lambda/\mathrm{d}\tau$, monotonically increases from $(2M-1)/M^2$ to $2/M$; the dimensionless temperature of the warm zone, θ, monotonically decreases from $M^2/(2M-1)$ to zero; and the dimensionless horizontal heat flux, Φ, (i.e. the ratio of the total horizontal flux, $\mu l F_l$, through the interface between zones W and B to the total vertical flux, lQ_s, incoming through the free surface of the zone W) monotonically increases from zero to unity.

Equations (41)–(43) and (45)–(48) contain one dimensionless constant C_t and one dimensionless parameter M including another constant C_M. The latter is the ratio of the bar-zone width to the basin depth in the zone. It is supposed to be of the order of unity. Then, if $\mu < 10^{-1}$, we can adopt $M = 1$ in all equations from (41) to (48), so that the exact value of C_M is not required. On the other hand, the solution depends considerably on C_t. The empirical estimate $C_t = 0.008$ will be obtained in the next section.

The solution of the problem (41), (42), (44) at $M = 1$ and $C_t = 0.008$ is shown on figure 5 below. It is obtained numerically using asymptotic expressions (45), (46) at small τ to avoid the singularity in the equations at $\tau = 0$. Sensitivity of the solution to the choice of C_t is as follows: the difference $\lambda - \tau$, i.e. the 'correction term' responsible for the dynamical warming effect on the acceleration of thermal-bar propagation, appears to be approximately linearly dependent on C_t.

4.2. *Laminar regime*

As mentioned in the Introduction, investigation of the laminar thermal bar is needed for proper interpretation of laboratory experiments. We are interested, first, in the transition from the laminar to the turbulent regime, which is why it is convenient in further considerations to keep the same scales and dimensionless variables as in §4.1, namely those determined by (39) and (40).

Then (16), (25), (35) take forms similar to (41), (42), with the one exception of the formula for the dimensionless horizontal dynamic heat flux, Φ. This is now expressed as

$$\Phi = \epsilon \lambda^2 \theta^3, \tag{49}$$

where ϵ is the following dimensionless number:

$$\epsilon = \frac{C_l^2 Q_s^3}{\nu g a \mu^3 (T_m - T_0)} \tag{50}$$

compiled from the external parameters.

From (41*a*), (42) and (49), the following equation is derived:

$$\left(M-\frac{\tau}{\lambda}\right)\frac{\mathrm{d}\lambda}{\mathrm{d}\tau}-\epsilon M^2\lambda^2\left(2\frac{\tau}{\lambda}-M\right)^3-\frac{M-1}{M}=0. \tag{51}$$

It should be integrated using the initial condition (44).

We analyse below the data from laboratory experiments (Elliott & Elliott 1970; Kreiman 1989). Typical values of governing parameters were: $\mu \approx 10^{-1}$, $Q_s \approx 10^{-2}$ K cm s^{-1}. Substituting these values into (50) and adopting the upper estimate of $C_l \ll 10^{-2}$ (which follows from Golitsyn's estimate of the constant $a_w \approx 9$ in (36)) we obtain $\epsilon \ll 10^{-5}$. This limitation permits a solution of the problem (51), (44) to be sought in the form of a power series in ϵ. Keeping the first two terms of such a series at $\tau \ll \epsilon^{-\frac{1}{2}}$, we obtain

$$\lambda \approx \frac{2M-1}{M^2}\tau+\frac{1}{4M-3}\epsilon\tau^3, \tag{52}$$

$$\theta \approx \frac{M^2}{2M-1}-\frac{2M^5}{(2M-1)^2(4M-3)}\epsilon\tau^2. \tag{53}$$

At $\mu < 10^{-1}$ we can take $M = 1$ here.

Solution of the problem under consideration at very high values of τ is of no interest since, as τ increases, the dimensionless distance λ, the water depth in the bar zone $d = \mu l_* \lambda$, and the Raleigh number Ra, determined by (37*a*), also increase. When Ra exceeds its critical value ($Ra \approx 10^6$), the thermal bar becomes turbulent. Then (34), (35) and all their consequences, including (51), no longer make physical sense.

The condition for turbulence, $Ra > Ra_t$, can be replaced by any one of the following inequalities:

$$d > d_t, \quad l > l_t = d_t/\mu, \quad \lambda > \lambda_t = d_t/\mu l_*, \quad \tau > \tau_t, \tag{54}$$

where d_t is the critical depth determined by (38) and τ_t is the critical dimensionless time. The latter can be obtained, at sufficiently small ϵ, as a root of the cubic equation

$$\frac{\epsilon}{4M-3}\tau_t^3+\frac{2M-1}{M^2}\tau_t-\lambda_t=0, \tag{55}$$

and at any ϵ, from the numerical solution of the problem (51), (44).

So, the thermal bar is laminar while $\tau < \tau_t$. Its movement is described by the solution of the problem (51), (44) or, approximately, by (52). At $\tau > \tau_t$, the bar becomes turbulent. Then its movement is governed by (43) which should be solved at the initial condition

$$\lambda = \lambda_t \quad \text{at} \quad \tau = \tau_t. \tag{56}$$

The dimensionless mean temperature of the warm zone, θ, is expressed by (42*a*) in both regimes.

5. Experimental data

The theoretical model of the *turbulent* thermal bar given above contains the dimensionless constant C_t. Our empirical estimate, used in §4, is based on very scanty information. The data from two lakes and two laboratory experiments, all that

Data source and reference	μ	$Q_s\left(\frac{\text{K cm}}{\text{s}}\right)$	T_0 (°C)	Δl	Δt	T_w (°C)
Ontario (Rodgers 1966)	3×10^{-3}	6×10^{-3}	2	11 km	10 days	4.9
Ladoga (Tikhmirov 1968)	2×10^{-3}	4×10^{-3}	0	17 km	33 days	6.4
Laboratory experiments	9×10^{-2}	9×10^{-3}	0	121 cm	65 min	6.2
(Elliott & Elliott 1969, 1970)	9×10^{-2}	12×10^{-3}	0	121 cm	52.5 min	—

TABLE 1. External parameters and measured characteristics of the thermal bar

Data source	l_* (cm)	t_* (s)	λ	θ	τ
Ontario	5144	5144	213	0.45	168
Ladoga	482	965	3527	0.60	2955
Laboratory experiments	0.0268	1.072	4515	0.55	3638
	0.0476	1.429	2542	—	2204

TABLE 2. Length- and timescales and dimensionless characteristics of the thermal bar

appeared to be available, are given in table 1. It includes the governing parameters, μ, Q_s and T_0, and the following observed characteristics of the thermal bar: the distance which it travelled, Δl, the time of its motion, Δt, and the mean temperature of the warm zone, T_w, achieved by the time the bar covered the distance Δl.

Table 2 presents evaluations based on the data of table 1, namely length- and timescales, l_* and t_*, and dimensionless variables, $\lambda = \Delta l/l_*$, $\theta = (T_w - T_m)/(T_m/T_0)$ and time, $\tau = \Delta t/t_*$, calculated using (39), (40).

In the graph of l versus t in Elliott & Elliott (1969, 1970) the initial moment of time corresponds to half an hour after the start of heating. Also, the cross-section of the experimental tank represents not a wedge but a trapezoid. Therefore, to interpret their experimental results in terms of our solution, we were obliged, first, to add 30 min to the time specified in the graph and, second, to consider as Δl the distance to the bar line from the imaginary origin of the wedge angle, rather than from the edge of the vessel (i.e. to add 11 cm to the distance specified on the graph).

Certainly there is no *a priori* confidence that the laboratory data correspond to the turbulent regime. Nevertheless, we plot them on figure 5 together with the lacustrine data from table 2 and the theoretical curves obtained from numerical solution of the 'turbulent problem' (41), (42), (44) at $M = 1$ and $C_t = 0.008$. This value of C_t is specified by fitting the $\lambda(\tau)$ curve to the Lake Ladoga point.

It is seen from the figure that the curve agrees fairly well with all other empirical points. So the final stage of the thermal bar development in the Elliott & Elliott (1969, 1970) laboratory experiment was probably turbulent. Equation (2) at large τ underestimates significantly the distance covered by the thermal bar. The $\theta(\tau)$ theoretical curve is quite well confirmed by two of the empirical points (corresponding to Lake Ladoga and laboratory experiments), while the Lake Ontario point lies much lower than the theoretical estimate. This disagreement may be caused by a comparatively small overestimate of initial temperature, T_0, in Lake Ontario.

Verification of the proposed theoretical model of the *laminar* thermal bar is based on the laboratory experiments of Kreiman (1989). The thermal bar was modelled in a wedge-shaped basin with a maximum depth of 15 cm and a tangent of the bottom inclination angle of $\mu = 0.107$ at different values of the heat flux Q_s. Temperature changes after switching on the heater were measured. The experiments were carried

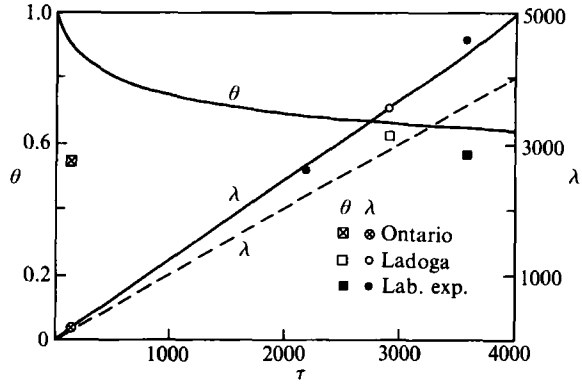

FIGURE 5. Dimensionless distance travelled by the bar, $\lambda = \Delta l/l_*$, and dimensionless warm-zone temperature, $\theta = (T_w - T_m)/(T_m - T_0)$, versus dimensionless time, $\tau = \Delta t/t_*$. Solid lines are plotted using the solution of the 'turbulent problem' (41), (42), (44) at $M = 1$ and $C_l = 0.008$; dashed line, using (2). Empirical points correspond to table 2.

Experiment no.	1	2	3	4	5	6
Q_s (10^3 K cm s^{-1})	3.3	4.7	5.1	5.5	5.4	5.9
$(T_m - T_0)$ (K)	1.7	1.3	2.0	2.4	1.5	2.0
t_* (s)	3.91	12.35	3.71	2.49	9.39	4.63
l_* (cm)	0.07	0.41	0.09	0.05	0.31	0.13

TABLE 3. External parameters and time- and lengthscales in laboratory experiments (Kreiman 1989)

out in late autumn. The windows in the laboratory hall were wide open, which kept the air temperature between 5 and 7 °C, close to the water temperature in the laboratory tank. The tank was made of wood, i.e. of heat-isolating material. All this minimized heat exchange through the tank bottom and side walls. A description of the laboratory apparatus and the measuring tools employed is given in Kreiman (1989), which also contains experimental data on the dependence of l on t in six experiments (see table 3).

The same data represented in terms of the dimensionless variables (40), i.e. the dependence of λ on τ, are shown in figure 6 together with the theoretical curves obtained from the numerical solution of (51), (44) taking the appropriate values of the dimensionless number ϵ. To determine ϵ in each experiment, it was necessary to ascertain the dimensionless constant C_l. Its optimum value, corresponding to the theoretical curves in figure 6, was $C_l = 1.2 \times 10^{-6}$.

The dotted line on figure 6 shows the 'turbulent solution', i.e. the solution of (43), (44) at $C_t = 0.008$. The overwhelming majority of the empirical points lie below the 'turbulent curve'. This is quite natural, because heat exchange between the W and B zones is obviously less effective in a laminar regime than in a turbulent one.

The dependence of θ on τ using the data of Kreiman's (1989) experiments and corresponding theoretical curves are represented in figure 7. Solid lines are obtained using (42*a*) and the solution of (51), (44) with $C_l = 1.2 \times 10^{-6}$; the dotted line is from the 'turbulent solution' at $C_t = 0.008$.

Now we can answer the second question concerning the value of laboratory experiments, namely how to distinguish the laminar and turbulent periods of

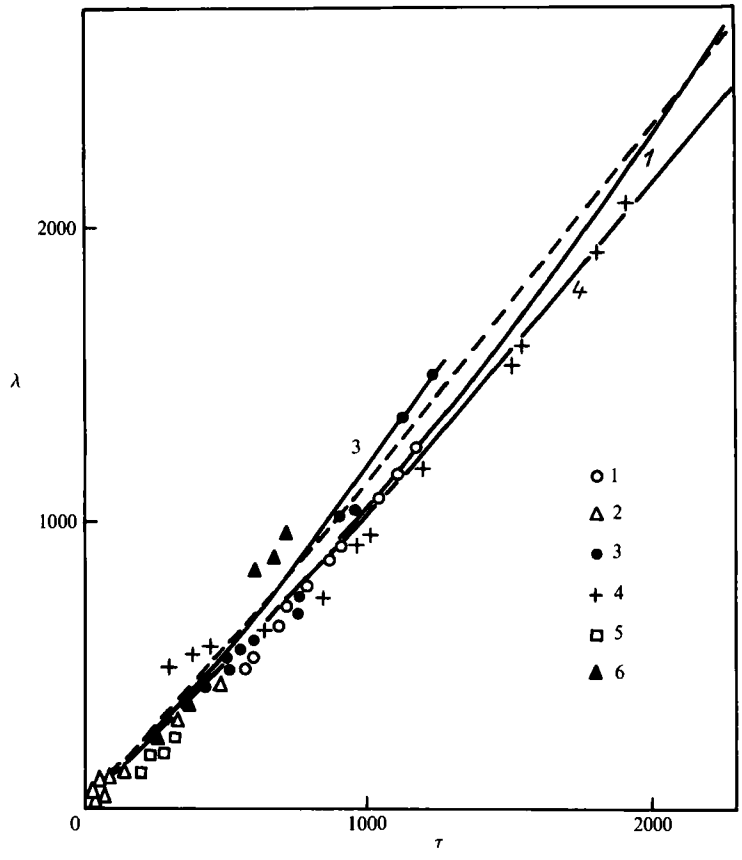

FIGURE 6. Dimensionless distance travelled by the thermal bar, $\lambda = l/l_*$, versus dimensionless time, $\tau = t/t_*$. Empirical points correspond to the data of laboratory experiments given in table 3. Solid lines are plotted using the solution of the 'laminar problem' (51), (44) at $C_t = 1.2 \times 10^{-6}$; dashed line, using the solution of the 'turbulent problem' at $C_t = 0.008$. Numbers at symbols and curves identify individual experiments.

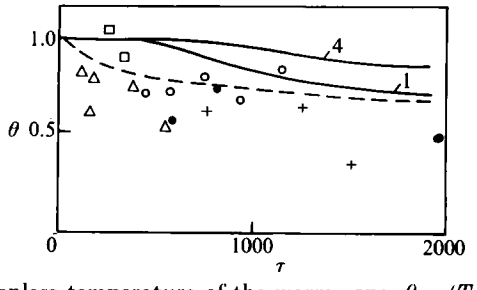

FIGURE 7. Dimensionless temperature of the warm zone, $\theta = (T_w - T_m)/(T_m - T_0)$, versus dimensionless time, τ. Notation is the same as in figure 6.

thermal bar development. The indication that the bar is becoming turbulent should be the coincidence of the empirical dependences of λ on τ and θ on τ with the theoretical 'turbulent curves'. Incidentally, according to this criterion, figure 5 shows that in the experiments of Elliott & Elliott (1970) the bar actually became turbulent.

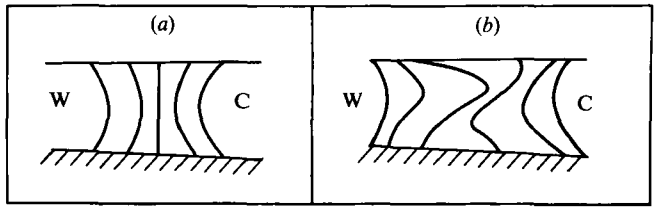

FIGURE 8. Schematic traces of sinking pigment particles: (*a*) at the 'slow', (*b*) at the 'fast' stage of thermal bar development.

Figure 8 shows schematically the results of visual observations on traces of sinking crystals of potassium permanganate which were dropped on the water surface in the course of the experiments. At the first 'slow' stage of propagation of the thermal bar, no noticeable asymmetry was observed between the circulation cells in the warm and cold regions (figure 8*a*). At the second, 'fast' stage starting 30–40 min from the beginning of an experiment, the frontal interface between the cells acquired an inclined position: a tongue of warm water slips onto the lower cold layer. In the process, the coloured traces acquired an S-shaped form (figure 8*b*) and started dissipating, especially near the free surface. This probably indicates the beginning of turbulence. Such a pattern fully conforms to the data on thermal bar propagation presented in figure 6: at the 'slow' stage ($\tau < 10^3$) there is no noticeable heating of the bar zone owing to the contact with the warm zone, so that $\lambda = \tau$. At the 'fast' stage, heating takes place, resulting in the acceleration of thermal bar propagation, so that $\lambda > \tau$. According to figure 8, this stage can be characterized as a laminar–advective one.

The most appropriate problems to solve by means of laboratory experiments similar to those carried out by Elliott & Elliott (1969, 1970) and Kreiman (1989) are as follows: (i) more precise determination of the universal constant C_t; (ii) determination of the critical Raleigh number for a thermal bar (we now use only an *a priori* estimate on the order of magnitude, $Ra_t \sim 10^6$); (iii) more careful examination of thermal bar propagation and, especially, the temporal behaviour of the warm-zone mean temperature. New experiments must be carried out in considerably deeper wedge-shaped tanks than before (with a maximum depth of at least 25–30 cm).

Further advancement in understanding the nature of the thermal bar requires extensive experimental work in lakes, including examination of temperature cross-sections and current systems *in situ* as well as remote sounding of the water surface temperature distribution.

The authors would like to thank Dr A. I. Tikhomirov for useful discussions and for his kind permission to reproduce his unpublished photograph of the thermal bar.

REFERENCES

BENNETT, J. R. 1971 Thermally driven lake currents during the spring and fall transition periods. In *Proc. 14th Conf. Great Lakes Res.*, pp. 536–544. Intl Assoc. Great Lakes Res.

CSANADY, G. T. 1970 On the equilibrium shape of the thermocline in a shore zone. Reprint, University of Waterloo, Ontario.

ELLIOTT, G. H. 1971 A mathematical study of the thermal bar. In *Proc. 14th Conf. Great Lakes Res.*, pp. 545–554. Intl Assoc. Great Lakes Res.

ELLIOTT, G. H. & ELLIOTT, J. A. 1969 Small-scale model of the 'thermal bar'. In *Proc. 12th Conf. Great Lakes Res.*, pp. 553–557. Intl Assoc. Great Lakes Res.

ELLIOTT, G. H. & ELLIOTT, J. A. 1970 Laboratory studies on the thermal bar. In *Proc. 13th Conf. Great Lakes Res.*, pp. 413–418. Intl Assoc. Great Lakes Res.

FOREL, F. A. 1880 La congelation des lacs suisses et savoyards pendant l'hiver 1879–1880, Lac Leman. *L'Echo des Alpes*, Geneve, vol. 3, pp. 149–161.

GOLITSYN, G. S. 1980 *Investigation of Convection with Geophysical Applications and Analogues.* Leningrad: Gidrometeoizdat Press, 56 pp.

HUANG, J. C. K. 1972 The thermal bar. *Geophys. Fluid Dyn.* **3**, 1–28.

HUBBARD, D. W. & SPAIN, I. D. 1973 The structure of the early spring thermal bar in Lake Superior. In *Proc. 16th Conf. Great Lakes Res.*, pp. 735–742. Intl Assoc. Great Lakes Res.

KREIMAN, K. D. 1989 Thermal bar after the data of laboratory experiments. *Okeanologiya* **29**, 935–938.

RODGERS, G. K. 1966 The thermal bar in Lake Ontario, spring 1965 and winter 1965–66. In *Proc. 9th Conf. Great Lakes Res.*, pp. 369–374. University of Michigan, Great Lakes Res. Div., Publ. 15.

RODGERS, G. K. 1968 Heat advection within Lake Ontario in spring and surface water transparency associated with the thermal bar. In *Proc. 11th Conf. Great Lakes Res.*, pp. 942–950. Intl Assoc. Great Lakes Res.

SUNDARAM, T. R. 1974 Transient thermal response of large lakes to atmospheric disturbances. In *Proc. 17th Conf. Great Lakes Res.*, pp. 801–810. Intl Assoc. Great Lakes Res.

TIKHOMIROV, A. I. 1959 On the thermal bar in Yakimvar Bay of Lake Ladoga. *Izv. Vsesoyuz. Geograf. Obshchestva* **91**, 424–438.

TIKHOMIROV, A. I. 1963 On the thermal bar of Lake Ladoga. *Izv. Vsesoyuz, Geograf. Obshchestva* **95**, 134–142.

TIKHOMIROV, A. I. 1968 Temperature regime and heat storage of Lake Ladoga. In *Thermal Regime of Lake Ladoga*, pp. 144–217. Leningrad University Press.

TIKHOMIROV, A. I. 1982 *Thermal Regime of Large Lakes.* Leningrad: Nauka Press, 232 pp.

TURNER, J. S. 1973 *Buoyancy Effects in Fluids.* Cambridge University Press, 367 pp.

ZILITINKEVICH, S. S. & KREIMAN, K. D. 1990 Theoretical and laboratory investigation of the thermal bar. *Okeanologiya* **30**, 223–230.

ZILITINKEVICH, S. S. & TERZHEVIK, A. YU. 1987 The thermal bar. *Okeanologiya* **27**, 732–738.

ZILITINKEVICH, S. S. & TERZHEVIK, A. YU. 1989 Correction to the Paper 'The Thermal Bar'. *Okeanologiya* **29**, 755–758.